Science Arts & Métiers (SAM)

is an open access repository that collects the work of Arts et Métiers Institute of Technology researchers and makes it freely available over the web where possible.

To cite this version :

Approximate analytical effective phase function obtained for a thin slab geometry

F. Vaudelle

Laboratoire LAMPA, Univ Bretagne Loire, Arts et Metiers ParisTech, 2 Boulevard du Ronceray, 49035 Angers cedex 01, France

k

A B S T R A C T

The reflection and transmission of light from a slab containing a turbid medium provide a scattering effective phase function from which the true optical anisotropy factor may not be always easily retrieved. From the statistical Poissonian theory and thanks to approximations about the optical path related to the first scattering events, a simplified relationship is established between angular phase function and ef-fective phase function. Therefore, with a modified Gegenbauer or a Two-Terms Henyey-Greenstein phase function, some adjustable analytic functions are proposed in order to fit the measurements linked to the true effective phase function. An efficiency of the approximate analytical function is proved, thanks to the light modelling by Monte Carlo method, for optical thickness lower or equal to 2. This is confirmed by comparisons of the anisotropy retrieval with other methods. Concerning applications, several fits were made on experimental effective phase functions corresponding to goniometric measurements from usual diffusing materials and biological tissues.

1. Introduction

The detection of the diffused light from turbid media interests a lot of scientific field, such as biomedical [1,2] and biovegetal [3], and also atmospheric [4] and oceanic [5] studies. The scattering modelling uses bulk parameters such as the absorption coefficient μ_a and the scattering coefficient μ_s [6]. The coefficients μ_a and μ_s are the probabilities for a photon to be absorbed or scattered per length unit, respectively. Another important parameter is the anisotropy coefficient g, from which the reduced scattering coefficient $\mu'_s = \mu_s(1-g)$ can be obtained [6]. The parameter g is the mean cosine of the angular deviation θ, while μ'_s represents the probability of an isotropic scattering event per length unit. The values of g and μ_s have both influences on light transport close to the injection point, whereas the value of μ'_s is sufficient to describe the light scattering far from the source [7–10]. When only μ_s is known, the value of g must be retrieved to simulate the light propagation. Moreover, when only μ'_s is known, the retrieval of μ_s needs the value of g. The computing of g linked to a turbid medium can be seen as an important task.

Note that very close to the source, the modelling of the photon transport asks more information than only g. Therefore, the probability density of angular deviation, called the angular phase function $p(\theta)$, is often directly searched with a goniometric measurement [11–18] on different kind of samples, such as diffusing liquids [13–16] or biological tissues [11,12,17,18]. This function is necessary for the simulations of various turbid media [19–24] (for instance blood sample [20], human skin [21], or fruit tissues

[22–24]). Moreover, it gives the anisotropy coefficient g and other interesting factors [25,26], such as the parameter $\gamma = (1-f_2)/(1-g)$ which uses the first two moments of the phase function, g and f_2 (see Eq. 3), and may inversely characterize the weight of the large angle backscattering events. A very small volume of turbid medium, in such a way that just one scattering event exists, allows to obtain $p(\theta)$ from the measurements of the intensities scattered I(θ). This geometrical condition corresponds to a threshold length $l \sim 1/\mu_s$ (i.e. a dimensionless length such as $l\mu_s \sim 1$). However, the geometrical form generally used for samples is the slab geometry, and its great transverse length does not permit to have a dimensionless length $l\mu_s$ equal to 1. Nevertheless, this single scattering event condition is approached for a thickness d such as $d\mu_s \ll 1$ [11], i.e. a very thin slab which cannot always be realized.

In fact, the normalized distribution I(θ) is an effective phase function, that characterizes the multi scattering events. The studies on the effective phase function have been reported by several investigations [16,27–32]. The numerical simulations of this effective phase function by Monte Carlo [16,27–29] or adding-doubling [30] methods depend on the choice of the angular phase function. These numerical methods give often accurate results, but either need a large computing time or may not be enough flexible. Therefore, analytical solutions have been considered in order to provide an estimated value of the anisotropy [16,27,31], or to retrieve angular phase function [32]. These analytical methods don't take into account the specific geometry of a slab.

In this paper, an approximate analytical solution is proposed to represent the effective phase function observed at the boundaries

of a thin slab having an optical thickness such as $d\mu_s \sim 0.5$–2.5. It is used to fit the effective phase functions simulated by Monte Carlo code, and a comparison of the retrieved anisotropy coefficient is performed with the ones given by other analytical methods. Moreover, the fit is also applied on several set of experimental data obtained from the literature.

2. Anisotropy computed from analytical solutions

The anisotropy can be retrieved from simple analytical solutions described below, which are related to a slab geometry (example: Kubelka-Munk solution) or not. The dimensionless optical length τ, used as parameter, is the product between the scattering coefficient μ_s and a length. This length refers either to the thickness of a slab (d), or the depth coordinate (z) or the path-length of the light (l) when the slab geometry is not taken into account to build the analytical solution. Afterward in the others sections, the optical lengths linked to d and l will be represented by τ and $\tau_{(n)}$, respectively.

2.1. Analytical theory of Kubelka-Munk

The Kubelka-Munk theory is the equation of radiative transport for only one dimension z. The slab geometry can be adapted to this theory if the illumination source is isotropic, without specular reflection [33]. From this assumption, the total reflectance $R_T = \int_{\pi/2}^{\pi} p_{eff}(\theta).\sin(\theta)d\theta$ and transmittance $T_T = \int_0^{\pi/2} p_{eff}(\theta).\sin(\theta)d\theta$ allow to consider the parameters of absorption $K = 2\mu_a = S(a\text{-}1)$ and scattering

$$S = \frac{3}{4}\mu'_s - \frac{1}{4}\mu_a = \frac{1}{bz} . \ln\left[\frac{[1-R_T(a-b)]}{T_T}\right] \tag{1}$$

where $p_{eff}(\theta)$ is the effective phase function, $a = 0.5(1+R_T^2\text{-}T_T^2)/R_T$, and $b = (a^2-1)^{1/2}$. For a slab of optical thickness τ, a thickness d, and for $\mu_a \ll \mu'_s$, the anisotropy coefficient can be estimated by

$$g_{KM} = 1 - \frac{4Sd}{3\tau} \tag{2}$$

2.2. Analytical solutions of the effective phase function

An angular phase function of a single scattering event can be seen through the formula:

$$p(\cos\theta) = \sum_{k=0}^{\infty} (2k+1)f_k P_k(\cos\theta) \tag{3}$$

where P_k are the Legendre polynomials and f_k are the characteristic moments. When the multi-scattering events are taken into account inside a turbid medium, the angular probability density has to be replaced by an effective phase function. A general analytical expression of the effective phase function, depending on the path-length l and the scattering coefficient μ_s (or the dimensionless path-length $\tau = \mu_s l$), has been established from two studies [27] and [32]. This solution is based on the radiative transport equation and on the Poissonian Compounds theory. The main difference between these two studies is the incorporation or not of the unscattered part, $\delta(\cos\theta-1)$, inside the function distribution. The expression of the effective phase function related to an optical length τ is then from [32]

$$p_{eff}^{(a)}(\tau,\cos\theta) = \sum_{k=0}^{\infty} (2k+1)e^{\tau(f_k-1)}P_k(\cos\theta) \tag{4}$$

or from [27]

$$p_{eff}^{(b)}(\tau,\cos\theta) = \sum_{k=0}^{\infty} (2k+1)\left(e^{\tau f_k}-1\right)(e^\tau-1)^{-1}P_k(\cos\theta) \tag{5}$$

where the relationship between these two distribution functions is

$$p_{eff}^{(a)}(\tau,\cos\theta) = (1-e^{-\tau})p_{eff}^{(b)}(\tau,\cos\theta) + e^{-\tau}\delta(\cos\theta-1) \tag{6}$$

From the simple solution $p_{eff}^{(a)}$, the anisotropy $g = f_1$ related to the optical path-length τ can be found by

$$g_a = \ln\left(\int p_{eff}^{(a)}(\tau,\mu)\mu d\mu\right)/\tau+1 \tag{7}$$

The solution $p_{eff}^{(a)}$ can be approached by the Henyey-Greenstein function when its parameter g is replaced by g^G with $G = [(\tau-1)e^\tau-1]/(e^\tau-\tau-1)$ [27] (moreover l is replaced by the depth z, i.e. $\tau \approx \mu_s z$). Therefore, another estimation of g is

$$g_b \approx \left[\int p_{eff}^{(b)}(\tau,\mu)\mu d\mu\right]^{1/G} \tag{8}$$

These solutions are based on the following property: the effective anisotropy $g^{(n)}$ of n scattering events is a product $g^{(n)} = \prod_{j=1 \to n} g(j)$, where $g(j)$ is the anisotropy of the scattering event (j). This rule is also available for any moment f_k. If $g(j)$ is a constant factor, then $g^{(n)} = g^n$. But the number of scattering events n and the optical thickness τ of a medium are often correlated, such as $\tau \sim n$. Owing to this approximation, another estimation of anisotropy has been suggested [31,16]

$$g_c \approx \left[\int p_{eff}(\tau,\mu)\mu d\mu\right]^{1/\tau} \tag{9}$$

These analytical approaches of the effective phase function do not take into account the influence of the boundaries of the medium, such as the ones of a slab geometry. The distribution of the single scattering event, occurring in a thin slab of optical thickness τ, was given by [34] and [35]:

$$p_1(\tau,\cos\theta < 0) = \frac{\cos\theta}{(1-\cos\theta)}p^{(1)}(\theta)[\exp(\tau/\cos\theta-\tau)-1] \tag{10}$$

$$p_1(\tau,\cos\theta > 0) = \frac{\cos\theta}{(1-\cos\theta)}p^{(1)}(\theta)[\exp(-\tau)-\exp(-\tau/\cos\theta)] \tag{11}$$

where $p^{(1)}(\theta)$ is an angular phase function, and with the assumption $\mu_a \ll \mu_s$. For a small thickness such as $\tau = 1/10$, these equations may be seen as the expression of the effective phase function, and can be used to retrieve the anisotropy coefficient.

In the next section, an approximate analytical solution of the effective phase function is proposed that takes into account the Poissonian Compounds theory linked to the multi-scattering and the slab geometry (with $1/10 < \tau < 2$). The goal is to use this analytical function to fit an experimental curve and to retrieve the anisotropy parameter.

3. Approximate analytical solution of the effective phase function in a slab

3.1. Statistical consideration

For the scattering events, the statistical approach can be used. In Fig. 1(a–c), the probability of n scattering events ($1 \leq n \leq 4$) according to the anisotropy is computed by Monte Carlo for a thin slab (300 μm) with an absorption coefficient $\mu_a = 0.01$ mm^{-1} and the use of a Henyey-Greenstein phase function [36]. The source
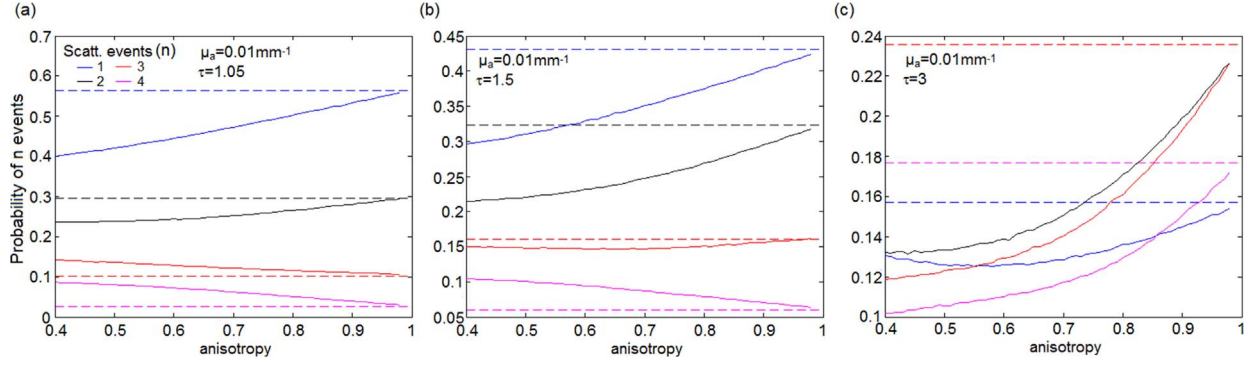
Fig. 1. Probabilities of n (1, 2, 3, and 4) scattering events (number of n scattering events/number of scattering events) versus anisotropy were computed thanks to Monte Carlo simulations made for a slab using a Henyey-Greenstein function, an absorption μ_a=0.01 mm^{-1} and according to an optical thickness of (a) τ=1.05, (b) τ=1.5, and (c) τ=3. The dotted lines show the values of $e^{-\tau}\tau^n/n!(1-e^{-\tau})^{-1}$.

(10^6 photons) illuminates normally the sample surface and there is no refractive index mismatch between the medium and the outside. The Monte Carlo code was established following the principles described by the Ref [19]. Particularly, a random variable ξ, $0 < \xi < 1$, is computed in such way that the integral of the angular density function is $\int_{-1}^{\cos\theta} p(\theta')d\cos\theta' = \xi$. Note that the azimuthal angle φ is chosen randomly between [0, 2π].

Three optical thicknesses are considered: τ=1.05, 1.5 and 3. For $\tau < 3$, the probabilities decrease with the number of events, while for τ=3 the probability of a single scattering event (n=1) is not the largest. Moreover, these probabilities are never constants with respect to the anisotropy coefficient. This is related to the influence of the angular deviation θ on the optical path inside the slab, and also illustrates that the distribution of scattering events linked to reflectance ($\cos\theta < 0$) is different of the transmittance one ($\cos\theta > 0$). Whatever the cases, the values of probability for anisotropy limit g_l=1 are $e^{-\tau}\tau^n/n!(1-e^{-\tau})^{-1}$, i.e. the Poisson probability of n order over the opposite probability of 0 event. Even if the Poissonian statistic may be applied for $g < 1$, the optical thickness has to be replaced by another dimensionless length, related to τ and $\cos\theta$, to define the mean of the Poisson statistic.

The Poissonian distribution can be associated with $p^{(n)}(\theta)$, the effective phase function of the nth scattering event, in order to give the distribution of the nth scattering event:

$$p_n(\tau,\cos\theta < 0) = p^{(n)}(\theta)\exp\left[-\tau_{(n)}(\tau,\cos\theta < 0)\right]\tau_{(n)}(\tau,\cos\theta < 0)^n/n! \quad (12)$$

$$p_n(\tau,\cos\theta > 0) = p^{(n)}(\theta)\exp\left[-\tau_{(n)}(\tau,\cos\theta > 0)\right]\tau_{(n)}(\tau,\cos\theta > 0)^n/n! \quad (13)$$

where $\tau_{(n)}(\tau, \cos\theta)$ is an optical path-length estimated and related to the nth scattering event. The effective angular phase function $p^{(n)}(\theta)$, which is related to the anisotropy coefficient g, is an angular phase function $p'(\theta)$ having as asymmetry parameter g^n. This assumption uses the principle previously cited ($g^{(n)}=g^n$), and has been validated by simulations using Henyey-Greenstein function till n~50 [29]. Note the fact that the distribution of the single scattering event n=1 has been already described by the Eqs. (10 and 11). Therefore, the Eqs. (12 and 13) concern only the order n > 1.

3.2. Approximation of the optical path-length

The dimensionless parameter $\tau_{(n > 1)}$ can be seen such as the dimensionless length linked to a schematic trajectory of a photon transport when there are at least two scattering events. For a scattering event n^{th}, $\tau_{(n)}$ should be dependent on several deflection angles $\theta_{(n)}$. But, as the approach used in [37], a scattering event can be related to a strong scattering (S), which modifies the direction, or to a forward scattering (F) for which the assumption $\tau/\cos\left(\theta_{(n)} - \theta_{(n-1)}\right) \sim \tau$ can be made. The series of these events (F, S) can be arranged in similar manner than a limited development, but differently with respect to the paths. The transmitted light may follow the distribution {1st event F or 1st event S, 2nd event F&S, 3th event S&F&F, etc…}, whereas the reflected part may follow {1st event S, 2nd event F &S, 3th event F&S&F, etc…}.

As long as there is only one event S, the dimensionless optical path can be described by two segments (see Fig. 2(a,b)). For a small optical thickness $\tau < 1$, the dimensionless length of these two segments is defined by $x\tau + x\tau/|\cos\theta|$ (reflectance case) or $x\tau + (1-x)\tau/|\cos\theta|$ (transmittance case), where $0 < x < 1$. In these conditions, $\tau_{(n > 1)}$ can be estimated by the average value of these dimensionless lengths $\tau_{(n > 1)} = <x\tau + x\tau/|\cos\theta|>_{x:0\to 1} = \int_0^1 [x\tau + x\tau/|\cos\theta|]dx$ or $\tau_{(n > 1)} = <x\tau + (1-x)\tau/|\cos\theta|>_{x:0\to 1} = \int_0^1 [x\tau + (1 - x)\tau/|\cos\theta|]dx$, and the two formulae give the same expression $\tau_{(n > 1)}=1/2(\tau + \tau/|\cos\theta|)$ (see Fig. 2(a)).

For an optical thickness $1 < \tau < 3$, $\tau_{(n > 1)}$ can be estimated with the help of the mean value of the first scattering event path-length $<\tau_{(n=1)}> = \tau_0$=1 [38]. If this first event is F, the optical depth of F&S (and F&S&F, F&F&S, F&S&F&F,.) can be approached by (see Fig. 2(b))

$$\tau_{(a)} \approx \tau_0 + x'(\tau - \tau_0) + (1-x')(\tau - \tau_0)/\cos\theta, (\cos\theta > 0, 0 < x' < 1) \quad (14)$$

or

$$\tau_{(b)} \approx \tau_0 + x'(\tau - \tau_0) + x'(\tau - \tau_0)/|\cos\theta| + \tau_0/|\cos\theta|, (\cos\theta < 0, 0 < x' < 1) \quad (15)$$

If the first event is S (see Fig. 2(b)), the optical depth of (S&F, S&F&F, S&F&F&F,.) can be approached by

$$\tau_{(c)} \approx x'\tau_0 + [(1-x')\tau_0 + (\tau - \tau_0)]/\cos\theta, (\cos\theta > 0, 0 < x' < 1) \quad (16)$$

The cases $\tau_{(a)}$, $\tau_{(b)}$, and $\tau_{(c)}$ were limited here to n=2, $2 \le n \le 4$, and $3 \le n \le 4$, respectively. By integrating x' between 0 and 1, several estimated optical depth $<\tau_{(n > 1)}(\tau,\cos\theta)>$ are obtained: for the transmittance case $\tau_{(3 \le n \le 4)}(\tau,\cos\theta > 0)=0.5 + (\tau - 0.5)/\cos\theta$; $\tau_{(n=2)}(\tau,\cos\theta > 0)=0.5(\tau + 1) + 0.5(\tau - 1)/\cos\theta$ (as shown in Fig. 2(c)), and for the reflectance case $\tau_{(2 \le n \le 4)}(\tau,\cos\theta < 0)=0.5(\tau + 1) + 0.5(\tau + 1)/|\cos\theta|$ (Fig. 2(d)).

3.3. Test with Henyey-Greenstein phase function

To validate the Eqs. (12) and (13) with the approximate dimensionless lengths Eqs. (14)–(16), a comparison was made with
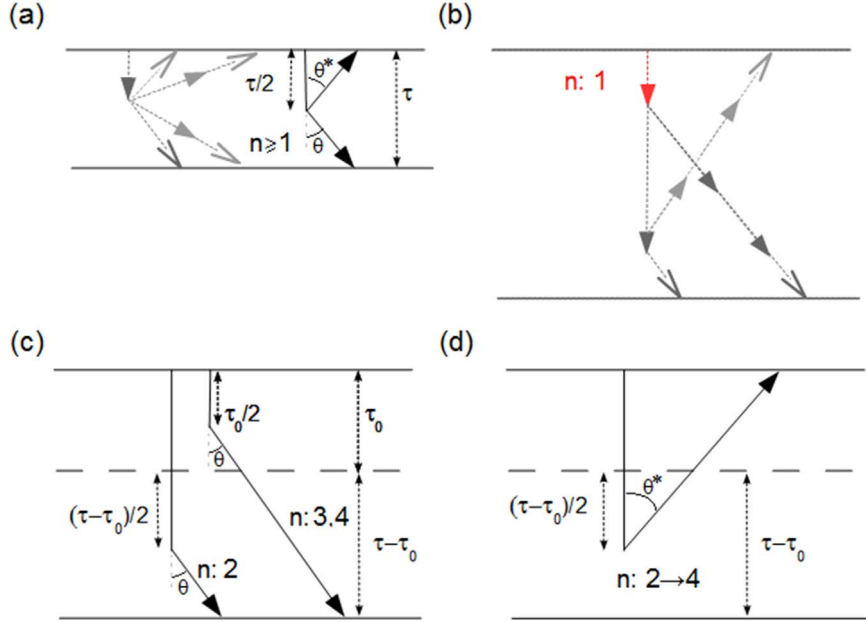
Fig. 2. Schema of dimensionless optical path length considered in this study. The black lines correspond to approximate and average path-lengths. (a) $\tau < 1$, (b) $\tau > 1$, path-lengths linked to the reflectance and transmittance cases. (c) $\tau > 1$, average path-length linked to transmittance case, (d) $\tau > 1$, average path-length linked to reflectance case. $\tau_0 = 1$ is the mean value of the first scattering event path-length.
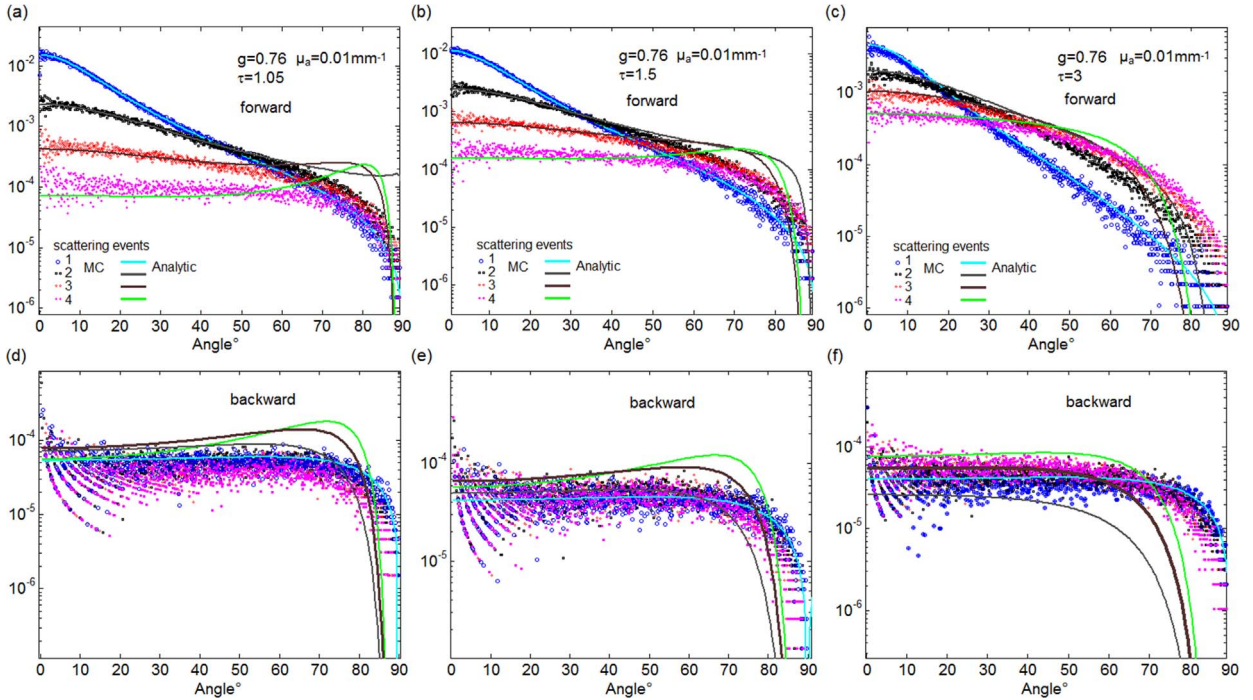

Fig. 3. For an anisotropy of 0.76, probabilities of n (1, 2, 3, and 4) scattering events versus the exit angle computed from either simulations described in Fig. 1 (symbols) or the approximate effective phase function Eqs. (12) and (13) (lines). (a) $\tau = 1.05$, (b) $\tau = 1.5$, and (c) $\tau = 3$.

the probabilities of n events, computed from the Monte Carlo simulations previously described in Section 3.1. Note that the quantity of exit photon captured over an angle θ_m (with an uncertainty of $\pm 0.05°$), when n iterations have been run, is proportional to the product between $\sin\theta_m \Delta\theta_m$ and the probability density function of n events. The Henyey-Greenstein functions p_{HG} used for the Eqs. (10)–(13) were such as $p^{(n)}(\theta) = p_{HG}^{(n)}(\theta, g) = p_{HG}^{(1)}(\theta, g^n)$, where g is the anisotropy coefficient. To perform the comparisons, two constants C_f and C_b have been multiplied to the

Eqs. (10)–(12) and (11)–(13), respectively. The case $g = 0.76$ is considered in the Fig. 3. It is shown the efficiency of the fits for θ inferior to 60°, especially for the forward part ($\cos\theta > 0$), and even till 90° concerning n=1. The error of fit is maximum for n > 1 around 80°.

Afterward, the use of the addition of Eqs. (12) and (13) to fit all the range of the measured angular distribution needs just one constant $C = C_f = C_b$ to be multiplied. It was found that the best compromise is to limit the order n till 3 regarding the forward

part. Therefore, an analytical phase function valid for a few scattering events may be given by:

$$p_{eff}(\tau,\cos\theta < 0) = p_1(\tau,\cos\theta < 0)$$
$$+ \sum_{n=2}^{4} p^{(n)}(\theta)\exp\left[-\tau_{(n)}(\tau,\cos\theta < 0)\right]\tau_{(n)}(\tau,\cos\theta < 0)^n/n! \tag{17}$$

$$p_{eff}(\tau, \cos\theta > 0) = p_1(\tau, \cos\theta > 0)$$
$$+ \sum_{n=2}^{3} p^{(n)}(\theta)\exp\left[-\tau_{(n)}(\tau, \cos\theta > 0)\right]\tau_{(n)}(\tau, \cos\theta > 0)^n/n! \tag{18}$$

Note that in the fitting algorithm, angles ranging from 75° to 115° were excluded for the error estimation.

3.4. Retrieval of the modified Gegenbauer phase function

The Henyey-Greenstein phase function is an empirical function who characterizes the angular distribution, but where the backward part is neglected compared to the forward part. Moreover, a high peak forward, often observed, cannot be accurately reproduced by this Henyey-Greenstein function. The improvement of this function has been proposed with the Gegenbauer function [39] or the modified phase functions [25,28,40] in order to take into account the peak-forward or the backward part, respectively. Adding a term proportional to $\cos^2\theta$ [25], the use of Two-Terms Henyey-Greenstein functions (called p_{TTHG}) [28] are examples of modified phase function. A modified phase function considered here is the modified Gegenbauer phase function:

$$p_{MGK}(\theta, g_{GK}, \alpha, f) = f\frac{\alpha g_{GK}}{\pi\left[\left(1+g_{GK}\right)^{2\alpha} - \left(1-g_{GK}\right)^{2\alpha}\right]}\frac{\left(1 - g_{GK}^2\right)^{2\alpha}}{\left(1+g_{GK}^2 - 2g_{GK}\cos\theta\right)^{\alpha+1}} + (1-f)$$
$$\times \frac{1}{4\pi}3\cos\theta^2 \tag{19}$$

where 3 parameters must be chosen. It should be noted that for $\alpha=0.5$, p_{MGK} gives the modified Henyey-Greenstein function p_{MHG} as the one defined by [25].

To incorporate partially this modified Gegenbauer function inside the Eqs. (17) and (18), several approximations can be made. The enhancement of the peak forward can be essentially observed for the first event (n=1). So even if $p^{(1)}(\theta)=p_{MGK}(\theta, g_{GK}, \alpha, f)$, the other functions $p^{(n)}(\theta)$ can always be built according to the Henyey-Greenstein functions. For $n > 1$ the parameter α of $p^{(n)}(\theta)$ is changed to 0.5, while g_{GK} is replaced by the power n of the anisotropy coefficient of $p_{MHG}(\theta,g_{GK},\alpha=0.5,f=1)$. Moreover, to be well adapted to the previously cited principles, i.e. Eq. (3) and $f_k^{(n)}(j)=\prod_{j=1\to n}f_k(j)$, the coefficient f and the term proportional to $\cos^2\theta$ must be modified for $n > 1$. It was found that $p^{(n)}(\theta)$ could be written for n superior to 1 such as

$$p^{(n)}(\theta) = f^n p_{MGK}(\theta, (g/f)^n, \alpha = 0.5, 1)$$
$$+ h_1(n, f, g)\frac{1}{4\pi}3\cos\theta^2 + h_2(n, f, g)\frac{1}{4\pi} \tag{20}$$

where g is the anisotropy coefficient of $p^{(1)}$:

$$g = f\frac{2g_{GK}\alpha\left[\left(1+g_{GK}\right)^{2\alpha} + \left(1-g_{GK}\right)^{2\alpha}\right]\Big/\left[\left(1+g_{GK}\right)^{2\alpha} - \left(1-g_{GK}\right)^{2\alpha}\right] - \left(1+g_{GK}^2\right)}{2g_{GK}(\alpha-1)} \tag{21}$$

and where $h_1(n,f,g)$ and $h_2(n,f,g)$ are:

$$h_1(n, f, g) = \frac{5}{2}\left(\left[fg^2 + 2/5\left(1-f\right)\right]^n - f^n g^{2n}\right) \tag{22}$$

$$h_2(n, f, g) = 1-f^n - \frac{5}{2}\left(\left[fg^2 + 2/5(1-f)\right]^n - f^n g^{2n}\right). \tag{23}$$

For a small value (1-f), $h_1(n,f,g)$ and $h_2(n,f,g)$ can be approximated by:

$$h_1(n, f, g) \approx nf^{n-1}(1-f)g^{2(n-1)} \tag{24}$$

$$h_2(n, f, g) \approx 1-f^n - nf^{n-1}(1-f)g^{2(n-1)}. \tag{25}$$

From the same principles (Eq. (3) and $f_k^{(n)}(j)=\prod_{j=1\to n}f_k(j)$), the Two-Terms Henyey-Greenstein phase function corresponding to an order n, $p_{TTHG}^{(n)}(\theta)$, has been already given in the study [28]. As made above, $p_{TTHG}^{(n)}(\theta)$ can also be approximated for a small value (1-f) by:

$$p_{TTHG}^{(n)}(\theta) \approx f^n p_{MGK}(\theta, (g/f)^n, \alpha = 0.5, 1) + nf^{n-1}(1-f)$$
$$p_{MGK}(\theta, (g/f)^{n-1}\cdot g_b, \alpha = 0.5, 1) \tag{26}$$

where g_b is a negative coefficient. Then, the approximate effective phase function using $p^{(n)}(\theta)$, defined by the Eqs. (20), (21), (24) and (25) or the Eqs. (21) and (26), may be used as analytical model for fit methods.

4. Results

4.1. Henyey-Greenstein phase function

With the same set of simulations as the one used in Section 3.1, several simulated effective phase functions I(θ) were considered according to different values of optical thickness (τ=0.6, 1.05, 1.2, 1.5, 1.8, 2.4, 3). With the help of Trust-Region method, the fits of I(θ) by analytical functions were performed. Fig. 4 shows different cases of fit with the fixed parameters α=0.5 and f=1. For an optical thickness of τ=0.6 and for g=0.86, the fit is made either by the phase function $p_1(\tau,\theta)$ Eqs. (10) and (11) or by the approximate effective phase function $p_{eff}(\tau,\theta)$ (Eqs. (17) and (18) for $\tau < 1$), as shown in Fig. 4(a) and (b), respectively. The best retrieval is given by the approximate function with a retrieved anisotropy 0.856 while the phase function $p_1(\tau,\theta)$ gives 0.8023. For an optical thickness larger than 1, the fits made with $p_{eff}(\tau,\theta)$ were correct till τ=2.4. Fig. 4(c) shows a good fit for τ=1.5, while in the Fig. 4(d) is plotted a fit with a lower correlation R²=0.96 obtained when τ=3.

In order to evaluate more precisely the efficiency of fit by the approximate effective phase function (Eqs. (17) and (18)) for $\tau > 1$, comparisons were made between the retrieved anisotropies obtained from the fit or from other analytical methods (Eqs. (7)–(9)). Fig. 5 shows that the retrieval of anisotropy made with the fit method is the best for $\tau < 2$. For $\tau > 2$, the anisotropies estimated by Eqs. (8) and (9) are better, especially for the Eq. (9). The error linked to the method of Eq. (8) is always limited whatever τ. The two other methods, Eqs. (2) and (7), are not efficient, except for the cases (τ=1, g=0.56) and ($\tau > 2$, g=0.86), respectively. It was also observed in Fig. 5 that the effective anisotropy $g_{eff} = \int I(\cos\theta)\cos\theta d\cos\theta / \int I(\cos\theta)d\cos\theta$ is a wrong estimation of the true anisotropy when $\tau \geq 1$.

4.2. Modified Gegenbauer phase function

Another set of simulations was made by Monte Carlo using different modified Gegenbauer angular phase functions (Eq. (19)). The measured effective distributions I(θ) were fitted by the approximate effective phase function with the use of Eqs. (20,21,24 and 25). Fig. 6 depicts several results obtained when τ=1.2, for f=1 (Fig. 6(a)–(b)) and f=0.9 (Fig. 6(c)–(d)). All the correlations R² of fit were superior to 0.99. The orders of magnitude of α and f estimated using p_{eff} were the same than the true ones used in the Eq. (19).
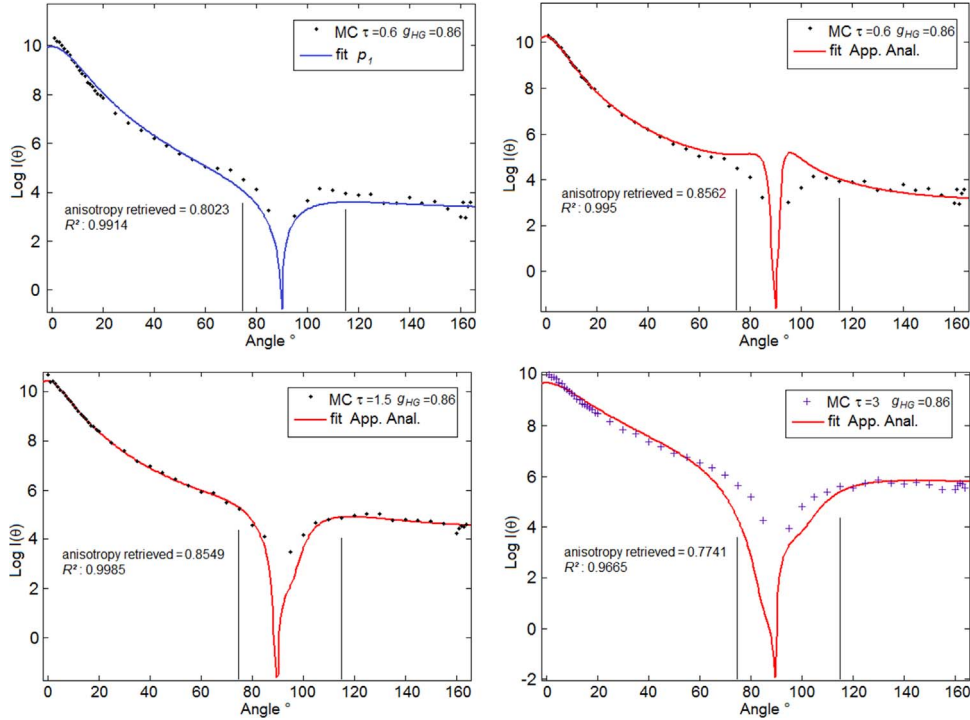
Fig. 4. Effective phase functions (semi-logarithm) obtained by simulations using Henyey-Greenstein function ($g=g_{HG}=0.86$). (a) Fit by Eqs. (10) and (11) with $\tau=0.6$. (b) Fit by Eqs. (17) and (18) with $\tau=0.6$. (c) Fit by Eqs. (17) and (18) with $\tau=1.5$. (d) Fit by Eqs. (17) and (18) with $\tau=3$. Fit correlation R^2 and retrieved anisotropy are shown.

A comparison of the retrieved anisotropies was performed between the computing methods (Eqs. (2),(8) and (9)) and the fit methods using either Eq. (20) (MGK) or Eq. (20) with α fixed to 0.5 (MHG). The results considered for three anisotropy categories (~ 0.56, ~ 0.7, ~ 0.86) are shown in Table 1. For $\tau=1.2$ and $f=1$, the fit by MGK gives low errors especially when $\alpha \neq 0.5$. The errors for the fits methods (MHG or MGK) increase when $0.85 < f < 1$, but are close to the ones obtained with the Eq. (8). Nevertheless, for a specific case ($f < 1$, $\alpha=0.5$ and $\tau=1.8$), the fit method shows errors smaller than the other methods. The Kubelka-Munk method (Eq. (2)) gives best results when $f < 1$ (for $\tau=1.2$), which can be explained by the fact that the Kubelka-Munk theory becomes more interesting when the angular asymmetry is reduced [41].

A good correlation R^2 of fit is obtained with the help of this approximate "effective" phase function when $\tau < 2$, which permits to retrieve efficiently the anisotropy coefficient. It can be used for different profile shapes with the use of a modified Gegenbauer function. Therefore, an application of this solution can be made on real measurements. In the next section several experimental

effective phase functions obtained from the literature are studied thanks to the analytical solutions.

4.3. Fit on experiments data

Several fits were made here on data based on experimental points copied from the studies [12,18,30]. First, the diffusions obtained from materials often used to build phantoms or be light diffusers [30] are tested with the fitting method. Then, biological tissues [12,18] are considered.

4.3.1. Fit on bulk diffusing materials

Two effective phase functions were measured by Leyre et al. [30] for two samples: TiO_2 particles inside silicone oil and LDPE (Low-Density PolyEthylene). The optical thickness of the slab containing the TiO_2 particles, estimated from the regular transmittance, was $\tau=0.85$, and the one of LDPE was $\tau=1.85$. Because all the angle range [0, 180°] is considered, a peak of backscattering around the region [160°–180°] appears for the two cases (Fig. 7).
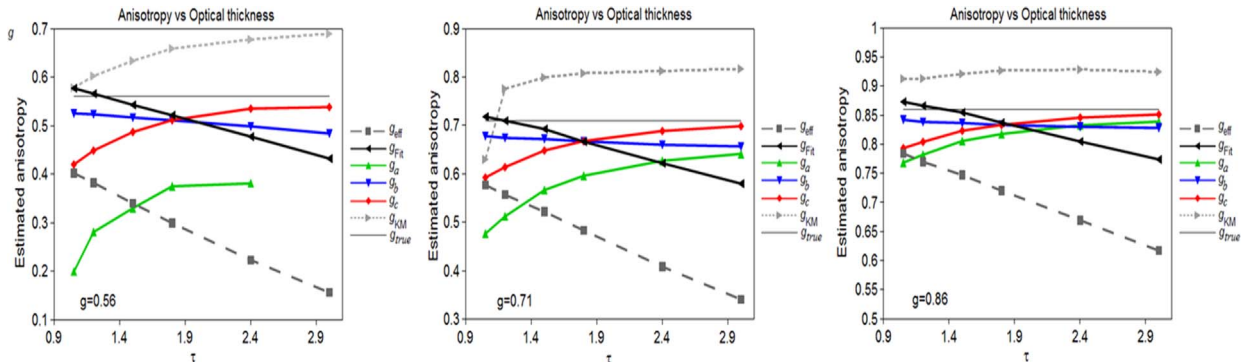

Fig. 5. Comparison between the retrieved anisotropies according to the optical thickness τ, when the true anisotropy g_{true} is 0.56 (a), 0.71 (b), and 0.86 (c). The effective phase function p_{eff} was Henyey-Greenstein and the absorption coefficient was 0.01 mm^{-1}. The retrieval methods were: the computing of the effective anisotropy (g_{eff}), the fit by the Eqs. (17) and (18) (g_{Fit}), the computing of the Eq. (2) (g_{KM}), Eq. (7) (g_a), Eq. (8) (g_b) and Eq. (9) (g_c).
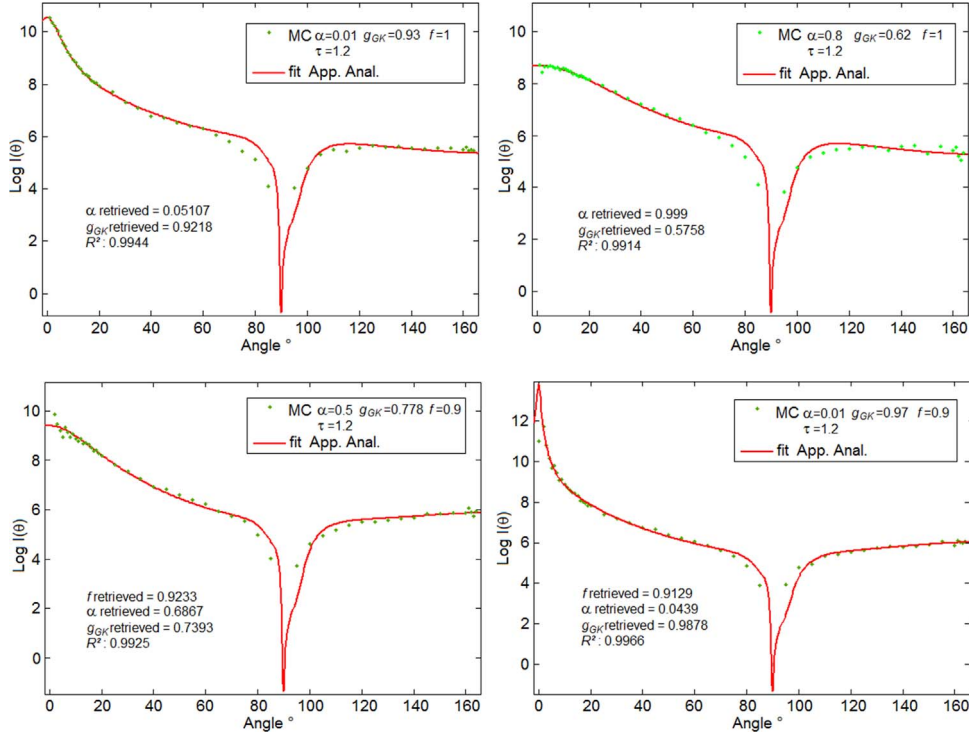
Fig. 6. Effective phase functions (semi-logarithm) obtained by simulations using modified Gegenbauer function (τ=1.2). Fit by Eqs. (17), (18) and (20) with (a) α=0.01, g_{GK}=0.93 and f=1. (b) α=0.8, g_{GK}=0.62 and f=1. (c) α=0.5, g_{GK}=0.778 and f=0.9. (d) α=0.01, g_{GK}=0.97 and f=0.9. Fit correlation R^2 and retrieved parameters are shown.

Table 1
Errors in the retrieval of anisotropy coefficient obtained thanks to fits using Eq. (20) with α=0.5 (*MHG*) or not (*MGK*), the computing of the Eq. (2) (g_{KM}), (8) (g_b), and (9) (g_c) and the computing of the effective anisotropy (g_{eff}).

τ	1-f	α	g true	Error Fit MHG	Error Fit MGK	Error g_{KM}	Error g_{eff}	Error g_b	Error g_c
1	0.15	0.5	0.56000	8.98%	13.20%	1.38%	26.61%	5.74%	26.68%
1	0.1	0.5	0.56000	6.85%	11.05%	1.40%	26.11%	5.28%	26.18%
1.2	0.1	0.5	0.56000	4.29%	8.32%	5.72%	31.85%	6.63%	19.98%
1.8	0.1	0.5	0.56000	4.80%	2.64%	16.99%	46.19%	8.40%	8.30%
1.2	0.05	0.001	0.56372	11.73%	8.53%	2.72%	31.83%	6.81%	20.05%
1.2	0.1	0.001	0.55919	13.27%	8.80%	3.32%	31.70%	6.45%	19.82%
1.2	0	0.8	0.56121	1.35%	0.80%	8.21%	31.90%	6.75%	20.06%
1.2	0	0.2	0.56286	5.12%	2.97%	6.49%	31.06%	6.06%	19.28%
1.2	0	0.001	0.56684	10.13%	3.26%	5.27%	30.57%	5.83%	18.89%
1	0.15	0.5	0.70000	7.57%	8.57%	0.97%	18.65%	4.68%	18.69%
1	0.1	0.5	0.70000	5.82%	7.81%	4.18%	18.31%	4.39%	18.36%
1.2	0.1	0.5	0.70000	3.62%	3.63%	7.46%	21.57%	4.59%	13.33%
1.8	0.1	0.5	0.70000	2.09%	2.21%	12.15%	32.82%	6.12%	6.06%
1.2	0.05	0.001	0.69881	10.09%	6.09%	4.38%	23.63%	6.23%	15.21%
1.2	0.1	0.001	0.69214	9.28%	10.44%	0.93%	25.52%	7.51%	16.82%
1.2	0	0.8	0.71040	2.34%	0.49%	10.56%	21.56%	5.04%	13.53%
1.2	0	0.2	0.70671	3.86%	0.25%	7.86%	21.23%	4.61%	13.15%
1.2	0	0.001	0.70811	8.28%	2.43%	6.29%	20.62%	4.18%	12.63%
1	0.15	0.5	0.86000						
1	0.1	0.5	0.86000	5.26%	6.73%	1.85%	12.00%	4.82%	12.03%
1.2	0.1	0.5	0.86000	4.48%	5.81%	0.40%	13.53%	4.74%	9.15%
1.8	0.1	0.5	0.86000	1.52%	2.40%	0.91%	18.29%	4.45%	4.42%
1.2	0.05	0.001	0.86238	2.44%	3.65%	5.55%	26.03%	14.32%	20.27%
1.2	0.1	0.001	0.86000						
1.2	0	0.8	0.86279	0.75%	0.89%	7.81%	10.21%	2.40%	6.31%
1.2	0	0.2	0.86747	2.01%	0.99%	4.70%	9.47%	2.03%	5.75%
1.2	0	0.001	0.86470	1.11%	3.21%	2.21%	12.69%	4.29%	8.50%

It can be explained by the effect of Fresnel reflection occurring at the surfaces.

First, the region [$\sim$160°–180°] was excluded from the estimation error concerning the fits made by Eqs. (17) and (18) and (20) (called fit 1 in Fig. 7(a)–(c)). For τ=0.85, the fit 1 of the data linked to the sample TiO$_2$ gave small coefficients f=0.75 and α=0.225. The retrieved anisotropy 0.56 was slightly inferior to the expected value $\sim$0.6. Concerning LDPE sample (τ=1.85), great values of coefficients $\alpha \sim$0.9, $f \sim$0.99 and $g_{GK} \sim$0.87 were computed. The order of magnitude of these parameters were close to those given by [30].
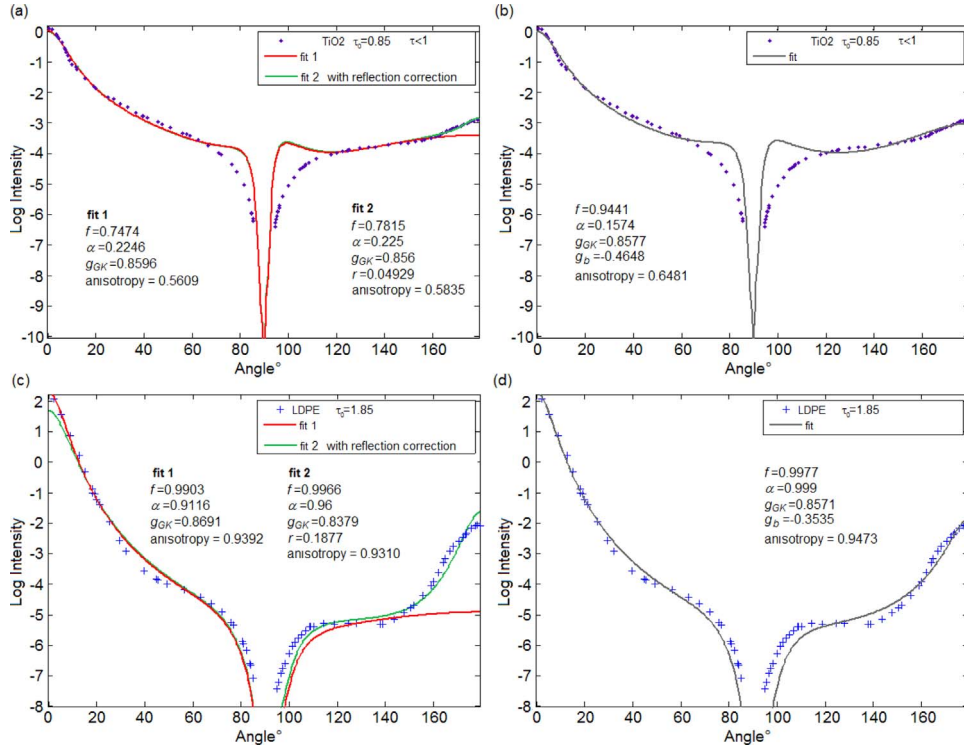
Fig. 7. Effective phase functions measured by [30]. (a) and (b): slab containing TiO2 (τ=0.85), (c) and (d) slab containing LDPE (τ=1.85). (a) and (c): Fit by Eqs. (17), (18) and (20) (Red lines) and by Eqs. (17), (18), (20) and (26) (Green lines). (b) and (d): Fit by Eqs. (17), (18) and (26) (Gray lines). The retrieved parameters are shown for each fit. (For interpretation of the references to color in this figure legend, the reader is referred to the web version of this article).
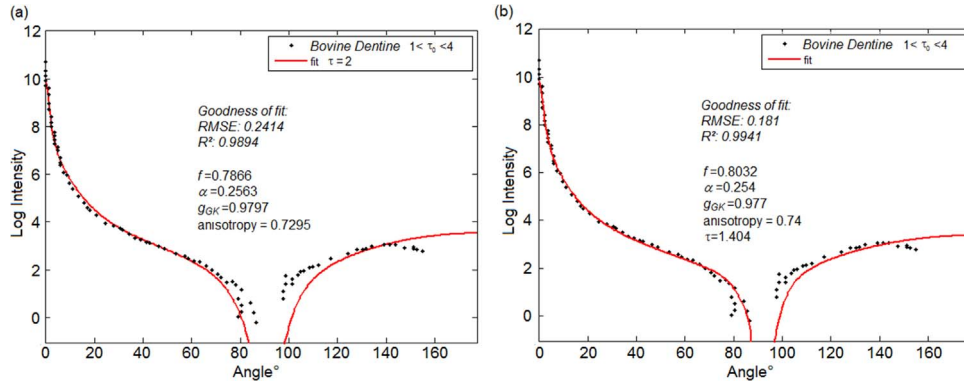

Fig. 8. Effective phase functions measured by [12]. Slab containing bovine dentine with tubules and measured light polarization parallel and perpendicular to plane of scattering, respectively. ($1 < \tau < 4$). (a) Fit by Eqs. (17), (18) and (20) for τ=2. (b) Fit by Eqs. (17), (18) and (20) for an optimized value of τ=1.404. The correlation R^2 and deviation RMSE of the fits, and the retrieved parameters are shown.
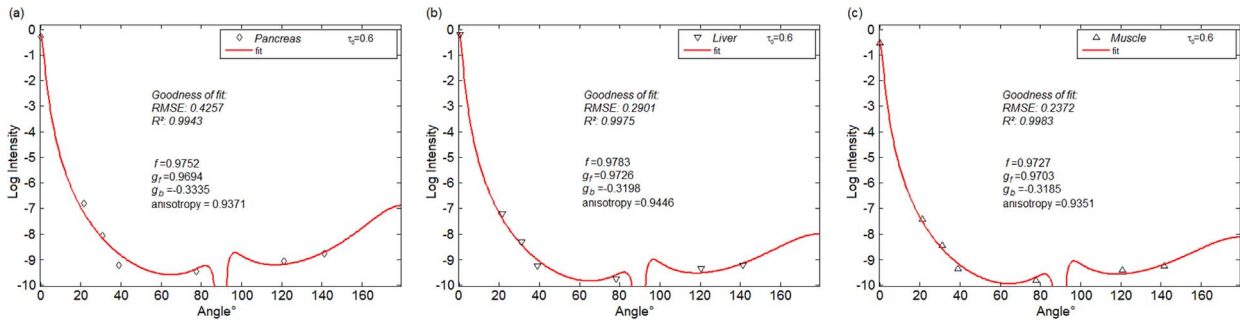

Fig. 9. Effective phase functions measured by [18]. Slabs containing tissue samples of (a) Pancreas, (b) Liver, and (c) Muscle (τ=0.6). Fit by Eqs. (17), (18) and (26) with α=0.5 fixed for $p^{(1)}$. The correlation R^2 and deviation RMSE of the fits, and the retrieved parameters are shown.

Second, in order to have a fit on the whole range of angle, a correction function was added to the reflectance part of the approximate solution (Eq. (17)):

$$p_{eff}^{corr}(\tau, \cos\theta < 0) = p_{eff}(\tau, \cos\theta < 0) + re^{-\tau}p_{eff}(\tau, -\cos\theta > 0, f=1) \quad (27)$$

where $p_{eff}(\tau, -\cos\theta > 0, f=1)$ is the Eq. (18), in using $-\cos\theta$ instead of $\cos\theta$, and where r is a new parameter that the Trust-Region algorithm has to search. With this corrected effective phase function, the fit of the points may be carried out up to 180° (fit 2 in Fig. 7(a)–(c)). The effects obtained on the retrieval of anisotropy were a slight increase ($+0.023$) and a very small decrease (-0.008) of values for the cases TiO_2 and LDPE, respectively. There is no improvement in the retrieval of anisotropy (~ 0.93) for the case LDPE with the corrected function Eq. (27).

If this strong backscattering peak is not seen as due to the Fresnel reflection on the slab surfaces, then the angular phase function related to the bulk material must take into account this effect. The function $p_{TTHG}^{(n)}(\theta)$ (Eq. (26)) can be used rather than the modified function. This angular phase function is able to yield a strong backscattering, especially around 180°. Fig. 7(b) and (d) depict the new fit obtained for TiO_2 and LDPE, respectively. The retrieved anisotropy linked to the case TiO_2 increases notably up to 0.65, while the one linked to LDPE remains close to 0.94.

4.3.2. Fit on biological tissues

Samples of bovine dentine (thickness ~ 19 μm) were studied at 633 nm by Zijp et al. [12]. The swine tissues ex vivo of pancreas, liver and muscle (thickness ~ 60 μm, $\mu_s \sim 100$ mm^{-1}) were studied at 1064 nm by Saccomandi et al. [18].

Regarding the bovine dentine, the scattering coefficient was estimated approximately by ~ 200 mm^{-1} or ~ 50 mm^{-1} according to [12] and [42], respectively. So the optical thickness τ may be between 1 and 3.8. The experimental profile used here was the one where the tubules and the light polarization were parallel and perpendicular to plane of scattering, respectively. First, a fit by Eqs. (17), (18) and (20) was made for $\tau=2$ (Fig. 8(a)). Second, another fit was performed where τ was considered as an unknown parameter to be found (Fig. 8(b)). The value of the retrieved optical thickness τ was 1.4. In both cases $\tau=2$ or 1.4, the parameters $f \sim 0.8$ and $\alpha \sim 0.25$ were small, giving an anisotropy ~ 0.73. Note that the anisotropies of bovine dentine estimated by [12], $\sim 0.4 \pm 0.1$, were obtained for a starting angle of $\sim 20°$ and with a Henyey-Greenstein model. With these limits, the fitting method provided a retrieved anisotropy of 0.57 for $\tau=2$, i.e. larger than the mean value 0.4.

Concerning the Liver, Pancreas, and Muscle tissues, the scattering light measurements were based on a specific goniometric technique, where only 7 angles are used. The functions $p_{TTHG}^{(n)}(\theta)$ were used in order to retrieve the same type of parameters ($g_{forward}$, $g_{backward}$ and f) as those considered in the study [18]. The fits were made with $\alpha=0.5$ and $\tau=0.6$, and the correlations R^2 obtained were larger than 0.99 (Fig. 9). The values of $g_{forward}$ (0.958, 0.964, 0.968) estimated from [18] by a fit with $p_{TTHG}^{(1)}(\theta)$ are close to those obtained by the Eqs. (17), (18) and (26) (0.969, 0.973, 0.970). But there are small gap between the sets of parameters g_b and f: ($g_b \sim -0.4, f \sim 0.90$) and ($g_b \sim -0.3, f \sim 0.97$) for the curves fitted with $p_{TTHG}^{(1)}(\theta)$ and $p_{eff}(\tau, \theta)$, respectively. That gives a difference of ~ 0.12 for the retrieved anisotropies. The value of the anisotropy found here for the liver (0.94) is close to the one found by [43] for porcine liver with a double integrating sphere and inverse Mote Carlo: 0.93.

5. Conclusion

The multi-scattering occurring in a slab prevents often the direct measurement of the phase function, even if the optical thickness is around 1. An effective phase function is proposed considering both the Poissonian statistic of the scattering events and an approximation of the optical path length. This analytical function depends on the optical thickness of the slab and on the choice of an angular phase function (such as Modified Gegenbauer, Modified Henyey-Greenstein or Two-Terms Henyey-Greenstein functions). This solution is tested with results obtained by Monte Carlo simulations and its efficiency to retrieve the anisotropy is compared with other analytical methods. The threshold of the approximation corresponds to an optical thickness of the slab less than 2.

The approximate effective phase function using Modified Gegenbauer or Two-Terms Henyey-Greenstein functions allows to study real intensity measurements related to a goniometric technique. Moreover, the perturbation of the Fresnel reflection due to the surfaces can be slightly corrected. Nevertheless, the choice of the angular phase function $p(\theta)$ inside the model may have a small effect on the retrieval of anisotropy coefficient. The fit with the approximate effective phase function is also made from intensity measurements related to biological tissues. The retrieved anisotropies can be compared with the ones obtained thanks to a fit with an angular phase function. As expected, the values of the estimated coefficient are larger when the effective phase function is used.

In conclusion, an analytical approached method is described here for the fast estimation of the anisotropy coefficients of turbid media, and also others parameters required for an angular phase function predefined, when the tissue thickness is around the value of mean free-path or slightly larger.

References

[1] Bashkatov A.N., Genina E.A., Tuchin V.V. Tissue optical properties. In: Handbook of Biomedical Optics, CRC Press; 2011, p. 67–100.

[2] Nasouri B Murphy TE and Berberoglu H. Near infrared laser penetration and absorption in human skin. In: Proceedings SPIE Mechanisms for Low-Light Therapy IX; 893207; 2014.

[3] Nicolaï B, Beullens K, Bobelyn E, Peirs A, Saeys W, Theran K, Lammertyn J. Non destructive measurement of fruit and vegetable quality by means of NIR spectroscopy: a review. PostHarvest Biol Technol 2007;46(2):99–118.

[4] Baran AJ, Furtado K, Labonnote L-C, Havemann S, Thelen J-C, Marenco F. On the relationship between the scattering phase function of cirrus and the atmospheric state. Atmos Chem Phys 2015;15:1105–1127.

[5] Mobley CD, Sundman LK, Boss E. Phase function effects on oceanic light fields. Appl Opt 2002;41(6):1035–1050.

[6] Ishimaru A. Diffusion of light in turbid material. Appl Opt 1989;28:2210–2215.

[7] Mourant JR, Boyer J, Hielsher AH, Bigio IJ. Influence of the scattering phase function on light transport measurements in turbid media performed with small source-detector separations. Opt Lett 1996;21:546–548.

[8] Wang V, Jacques SL. Source of error in calculation of optical diffuse reflectance from turbid media using diffusion theory. Comput Methods Prog Biomed 2000;61(3):163–170.

[9] Kienle A, Forster FK, Hibst R. Influence of the phase function on determination of the optical properties of biological tissue by spatially resolved reflectance. Opt Lett 2001;26:1571–1573.

[10] Reif R, A'Amar O, Bigio IJ. Analytical model of light reflectance for extraction of the optical properties in small volumes of turbid media. Appl Opt 2007;46:7317–7328.

[11] Jacques SL, Alter CA, Prahl SA. Angular dependence of HeNe Laser light scattering by human dermis. Laser Life Sci 1987;1:309–334.

[12] Zijp JR, ten Bosch JJ. Angular dependence of HeNe-laser light scattering by bovine and human dentine. Arch Oral Biol 1991;36:283–289.

[13] Choukeife J, L'Huillier JP. Measurements of scattering effects within tissue-like media at two wavelengths of 632.8 nm and 680 nm. Lasers Med Sci 1999;14:286–296.

[14] Chicea D, Chicea LM. On light scattering anisotropy of biological fluids (urine) characterization. Rom Journ Phys 2007;52:383–388.

[15] Michels R, Foschum F, Kienle A. Optical properties of fat emulsions. Opt Express 2008;16:5907–5925.

[16] Hall G, Jacques SL, Eliceiri KW, Campagnola PJ. Goniometric measurements of thick tissue using Monte Carlo simulations to obtain the single scattering anisotropy coefficient. Biol Opt Express 2012;3(11):2707–2719.

[17] Fernandez-Oliveras A, Rubino M, Perez MM. Scattering anisotropy

measurements in dental tissues and biomaterials. J Eur Opt Soc Rap Public 2012;7:12016.

[18] Saccomandi P, Vogel V, Bazrafshan B, Maurer J, Schena E, Vogl TJ, Silvestri S, Mäntele W. Estimation of anisotropy coefficient of swine pancreas, liver and muscle at 1064 nm based on goniometric technique. J Biophotonics 2015;8 (5):422–428.

[19] Wang LH, Jacques SL, Zheng LQ. MCML-Monte Carlo modeling of light transport in multilayered tissues. Comput Methods Prog Biol 1995;47(2):131–146.

[20] Yaroslavsky AN, Yaroslavsky IV, Goldbach T, Schwarzmaier HJ. Influence of the scattering phase function approximation on the optical properties of blood determined from the integrating sphere measurements. J Biomed Opt 1999;4:47–53.

[21] Baranoski GVG, Krishnaswamy A, Kimmel B. An investigation on the use of data-driven scattering profiles in Monte Carlo simulations of ultraviolet light propagation in skin tissues. Phys Med Biol 2004;49:4799–4809.

[22] Watté R, Aernouts B, Van Beers R, Herremans E. Tri Ho Q., Verboven P., Nicolaï B., and Saeys W. Modeling the propagation of light in realistic tissue structures with MMC-fpf: a meshed Monte Carlo method with free phase function. Opt Express 2015;23:17467–17486.

[23] Vaudelle F, L'Huillier JP. Influence of the size and skin thickness of apple varieties on the retrieval of internal optical properties using Vis/Nir spectroscopy: a Monte Carlo-based study. Comput Electron Agric 2015;116:137–149.

[24] Askoura ML, Vaudelle F, L'Huillier JP. Numerical study of light transport in apple models based on Monte Carlo simulations. Photonics 2016;3:2.

[25] Bevilacqua F, Depeursinge C. Monte-Carlo study of diffuse reflectance at source detector separations close to one transport mean free path. JOSA A 1999;16:2935–2945.

[26] Bodenschatz N, Krauter P, Liemert A, Kienle A. Quantifying phase function influence in subdiffusively backscattered light. J Biomed Opt 2016;21 (3):035002.

[27] Turcu I. Effective phase function for light scattered by blood. Appl Opt 2006;45:639–647.

[28] Pfeiffer N, Chapman GH. Successive order, multiple scattering of two-term Henyey-Greenstein phase functions. Opt Express 2008;16:13637–13642.

[29] Piskozub J, McKee D. Effective scattering phase functions for the multiple scattering regime. Opt Express 2011;19:4786–4794.

[30] Leyre S, Meuret Y, Durinck G, Hofkens J, Deconinck G, Hanselaer P. Estimation of the effective phase function of bulk diffusing materials with the inverse adding-doubling method. Appl Opt 2014;53(10):2117–2125.

[31] Chicea D, Turcu I. Testing a new multiple light scattering phase function using RWMCS. J Optoelectron Adv Mat 2006;8:1516–1519.

[32] Le Bihan N, Margerin L. Nonparametric estimation of the heterogeneity of a random medium using Compound Poisson Process modeling of wave multiple scattering. Phys Rev E 2009;80:016601.

[33] Yust BG, Mimun LC, Sardar DK. Optical absorption and scattering of bovine cornea, lens, and retina in the near-infrared region. Laser Med Sci 2012;27:413–422.

[34] van de Hulst HC. Multiple light scattering.. New York: Academic Press; 1980.

[35] Prahl SA. Light transport in tissue [Thesis]; 1988.

[36] Henyey LG, Greenstein JL. Diffuse radiation in the galaxy. Astrophys J 1941;93:70–83.

[37] Desjardins AE. Angularly resolved backscattering of light from turbid suspensions of dielectric spheres. J Quant Spect Rad Transf 2006;102:139–151.

[38] DiRocco HO, Iriarte DI, Pomarico JA. Light propagation in turbid media: a generalization of the solution given by the diffusion approximation, based on the moments of multiple scattering. J Quant Spect Rad Transf 2010;111:2558–2561.

[39] Reynolds LO, McCormick NJ. Approximate two-parameter phase function for light scattering. JOSA 1980;70:1206–1212.

[40] Calabro KW, Bigio IJ. Influence of the phase function in generalized diffuse reflectance models: a review of current formalisms and novel observations. J Biomed Opt 2014;19(7):75005.

[41] Cheong WF, Prahl SA, Welch AJ. A Review of the Optical Properties of Biological Tissues. IEEE J Quant Elect 1990;26:2166–2185.

[42] ten Bosch JJ, Zijp JR. Optical properties of dentin. In: Thylstrup A, Leach SA, Qvist V, editors. Dentine and Dentine Reactions in the Oral Cavity. Oxford, England: IRL Press; 1987. p. 59–65.

[43] Ritz JP, Roggan A, Isbert C, Mueller G, Bhur HJ, Germer CT. Optical properties of native and coagulated porcine liver tissue between 400 and 2400 nm. Laser Surg Med 2001;29:205–212.